Contents lists available at ScienceDirect

# Physics Letters B

www.elsevier.com/locate/physletb



# The $\rho$ -resonance from $N_f=2$ lattice QCD including the physical pion mass



Matthias Fischer a,b, Bartosz Kostrzewa c, Maxim Mai d, Marcus Petschlies a,b, Ferenc Pittler e, Martin Ueding a,b, Carsten Urbach a,b,\*, Markus Werner a,b (Extended Twisted Mass Collaboration)

- <sup>a</sup> Helmholtz Institut für Strahlen- und Kernphysik, University of Bonn, Nussallee 14-16, 53115 Bonn, Germany
- <sup>b</sup> Bethe Center for Theoretical Physics, University of Bonn, Nussallee 12, 53115 Bonn, Germany
- <sup>c</sup> High Performance Computing & Analytics Lab, University of Bonn, Friedrich-Hirzebruch-Allee 8, 53115 Bonn, Germany
- <sup>d</sup> The George Washington University, Washington, DC 20052, USA
- <sup>e</sup> Computation-Based Science and Technology Research Center, The Cyprus Institute, 20 Kavafi Str., Nicosia 2121, Cyprus

#### ARTICLE INFO

#### Article history:

Received 19 August 2020 Received in revised form 28 May 2021 Accepted 9 June 2021 Available online 16 June 2021 Editor: B. Grinstein

#### ABSTRACT

We present a lattice computation of  $\pi\pi$ -scattering in the I=1 channel with  $N_f=2$  dynamical quark flavours obtained with ensembles bracketing the physical value of the pion mass. Employing a global fit to data at three values of the pion mass, we determine the universal parameters of the  $\rho$ -resonance. We carefully investigate systematic uncertainties by determining energy eigenvalues using different methods and by comparing inverse amplitude method and Breit-Wigner type parametrizations. Overall, exploring the complex energy plane we find mass  $M_{\rho}=786(22)$  MeV and width  $\Gamma_{\rho}=180(6)$  MeV, including statistical and systematic uncertainties. In contrast to previous  $N_f=2$  extrapolations from higher than physical pion mass results, our mass value is in good agreement with experiment, while the width is too high.

© 2021 The Author(s). Published by Elsevier B.V. This is an open access article under the CC BY license (http://creativecommons.org/licenses/by/4.0/). Funded by SCOAP<sup>3</sup>.

# 1. Introduction

Quantum Chromodynamics (QCD) – the theory of strong interactions – gives rise to a fascinating plethora of hadronic states: mesons and baryons. A theoretical understanding of these states from first principles requires a non-perturbative method, as provided by lattice QCD. As most of the hadrons are not stable under the strong interaction and decay, such an investigation must include resonance and interaction parameters.

One very prominent such state is the so-called  $\rho$ -resonance ( $\rho(770)$ ), which decays predominantly in a p-wave into two pions with isospin I=1. It is experimentally observed as a peak in cross-sections at an energy of  $M_{\rho} \sim 775$  MeV with width  $\Gamma_{\rho} \sim 150$  MeV [1]. The corresponding p-wave phase-shift curve is a prime example for a resonance phase-shift, see Refs. [2,3]. Via vector meson dominance, the  $\rho$  plays a fundamental role in our theoretical understanding of many processes [4] and, since it is well investigated experimentally, it represents a benchmark resonance state for lattice QCD simulations.

\* Corresponding author. E-mail address: urbach@hiskp.uni-bonn.de (C. Urbach).

The  $\rho$ -resonance has been investigated in lattice QCD previously [5–14], most recently in Ref. [15] with  $N_f = 2 + 1 + 1$  quark flavours including a continuum and chiral extrapolation. The latter was needed because the lattice simulations were performed at unphysically large values of the pion mass. One of the interesting conclusions from Ref. [15] is that the chiral extrapolation is difficult, even though there is guidance from effective field theories. The main reason for this was the lack of ensembles with sufficiently light pion mass, the lightest being at 230 MeV. For  $N_f = 2$ there is, most notably, one investigation with nearly physical pion mass value [9]. This calculation has been performed at a single lattice spacing value and one infinite volume pion mass value of about 150 MeV, finding an  $M_{\rho}$  value from a Breit-Wigner fit which is about 50 MeV below the experimental value mentioned above. Also their width is about 40 MeV below the experimental value, though the difference is covered by their estimate of the statistical

More recently, there is an ongoing discussion about the origin of the surprisingly large difference between the  $\rho$ -resonance parameters so far obtained in  $N_f=2$  and  $N_f=2+1(+1)$  flavour lattice QCD calculations [12,16–19].

**Table 1** Parameters and pion mass values of the ensembles used. All ensembles have  $\beta=2.10$  and clover coefficient  $c_{\rm SW}=1.57551$  in common. The first column corresponds to the ensemble tag used in the literature. For easier readability we will use the name given in the second row for this paper.

Tag [20]	Ens	$(L/a)^3 \times T/a$	N <sub>conf</sub>	$M_{\pi}$ [MeV]
cA2.09.48	E132	$48^{3} \times 96$	1485	132
cA2.30.48	E240	$48^{3} \times 96$	343	240
cA2.60.32	E340	$32^{3} \times 64$	334	340

With this letter we fill the gap to realistic pion mass values by including an ensemble slightly below the physical point. We present  $\rho$ -resonance parameters determined on three  $N_f = 2$ lattice QCD ensembles generated by the Extended Twisted Mass Collaboration (ETMC) [20] with pion masses between 132 and 340 MeV. Thus, we bracket the physical point with our ensembles. The ensemble at 132 MeV pion mass allows us in principle to directly determine the  $\rho$ -resonance phase shift in a model independent way using Lüscher's method. However, since Lüscher's method is only valid below the inelastic threshold, we have only five points available. This complication, which any lattice computation at the physical point will have to face, can be overcome by including heavier than physical pion mass ensembles in the analysis. We perform this analysis using the so-called inverse amplitude method [21-23] (IAM) at next-to-leading order in chiral perturbation theory, which is regularisation scale independent and preserves unitarity. In addition, we consistently incorporate the scale setting in our analysis and carefully estimate statistical and systematic uncertainties.

Moreover, by comparing to other lattice investigations we can shed new light on the question of the importance of the  $\bar KK$  threshold – which is not present in our calculation – for the  $\rho$ -resonance phase-shift.

#### 2. Lattice computation

The results for the  $\rho$ -resonance properties presented in this letter are based on gauge configurations generated by the ETMC at a single value of the lattice spacing, a=0.0914(15) fm [20]. These employ the Iwasaki gauge action [24] and two dynamical mass-degenerate flavours of Wilson twisted mass clover fermions at maximal twist [25,26]. With this action, physical quantities are  $\mathcal{O}(a)$  improved [27] such that discretisation effects only appear at order  $a^2$  in the lattice spacing. The three ensembles considered for this letter are compiled in Table 1 together with the lattice volume  $(L/a)^3 \times T/a$ , the number of configurations  $N_{\rm conf}$  used in this analysis and the pion mass value in physical units. For more details we refer to Ref. [20].

On these ensembles, we compute centre-of-mass energy levels  $E_{\rm cms}^{\Gamma}$  for irreducible representations (irreps)  $\Gamma$  of the lattice rotational symmetry group. We follow the procedure detailed in Ref. [15] and compute Euclidean correlation matrices  $\mathcal{C}_{\Gamma,\mathbf{p}^2}$ 

$$C_{\Gamma, \mathbf{p}^2}(t) = \langle \mathcal{O}_{\Gamma, \mathbf{p}}(t' + t) \cdot \mathcal{O}_{\Gamma, \mathbf{p}}(t')^{\dagger} \rangle \tag{1}$$

averaging over all equivalent momenta  $\mathbf{p}$ . The operators  $\mathcal{O}_{\Gamma,\mathbf{p}}=(\mathcal{O}_{\Gamma}^1,\mathcal{O}_{\Gamma}^2,\ldots)^t$  are chosen to project to irrep  $\Gamma$  for total squared momentum  $\mathbf{p}^2$ . The list of irreps  $\Gamma$  considered is  $T_{1u}$ ,  $A_1$ , E,  $B_1$ ,  $B_2$  up to  $\mathbf{d}^2=4$  with  $\mathbf{p}=2\pi\mathbf{d}/L$ .

The basis operators used to construct the operators  $\mathcal{O}_{\Gamma,\mathbf{P}}$  are two pion and single vector meson operators

$$\mathcal{O}_{\pi^{+}\pi^{-}}(x,y) = \bar{d}i\gamma_{5}u(x)\bar{u}i\gamma_{5}d(y),$$

$$\mathcal{O}_{\rho}(x) = \frac{1}{\sqrt{2}}(\bar{u}\Gamma^{\rho}u(x) - \bar{d}\Gamma^{\rho}d(x))$$
(2)

with  $\Gamma^{\rho} \in \{i\gamma_i, \gamma_0\gamma_i\}.$ 

We apply the generalised eigenvalue method (GEVM), i.e., solve the generalised eigenvalue problem [28,29]

$$C_{\Gamma, \mathbf{p}^2}(t)\eta^{(n)}(t, t_0) = \lambda^{(n)}(t, t_0)C_{\Gamma, \mathbf{p}^2}(t_0)\eta^{(n)}(t, t_0)$$
(3)

for eigenvalues  $\lambda^{(n)}(t,t_0)$  and eigenvectors  $\eta^{(n)}$ , where n labels the contributing states. Energy levels of these can be determined from the exponential fall-off of  $\lambda^{(n)}(t,t_0)$  at large t with  $t_0$  fixed. In addition, we apply the so-called Prony generalised eigenvalue method (PGEVM) in form of a matrix pencil on top of the GEVM [30] to reduce excited state contaminations.

The confidence in our energy eigenvalue extractions is increased by employing the following three methods:

**A1**: direct fit to each  $\lambda^{(n)}(t,t_0)$  using a fit range chosen by eye.

**A2**: direct fit to each  $\lambda^{(n)}(t,t_0)$  using the fit range which yields the fit with the best *p*-value.

**A3:** fit to the principal correlator of the PGEVM obtained from  $\lambda^{(n)}(t,t_0)$  [30] using a fit range chosen by eye.

Energy eigenvalues for which the three methods do not yield consistent results are discarded. To account for residual deviations, we perform the resonance parameter determinations based on energy eigenvalues obtained using each method separately and take the maximal difference between the resulting parameter values as a systematic uncertainty.

When considering multi-particle operators with periodic boundary conditions, the corresponding correlation functions are polluted by contributions from so-called thermal states and there exist several methods to reduce or remove these. However, in Ref. [15] we have shown that in the I=1 channel, the extracted energies agree within errors with or without thermal state subtraction if the fit-range is chosen carefully. We have checked that this is the case also here and thus use energy levels extracted without thermal state subtraction. Like in Ref. [15], we use so-called stochastic Laplacian Heaviside smearing [31] with algorithmic parameters identical to Ref. [32]. For the determination of the pion decay constant on the same gauge configurations, we also employ local time slice sources and the so-called one-end-trick, for details see Ref. [33].

#### 3. Phase-shift determination

The discrete and real valued lattice energy levels  $E_{\rm cms}^{\Gamma}$  are mapped to the infinite volume scattering quantities using Lüscher's method [29,35,36]. In case of the  $\rho$ -meson and under the assumption that higher partial waves can be neglected, the p-wave phaseshift  $\delta_1$  is related to the energy levels via

$$\cot \delta_1 = M^{\Gamma}(k^2) \,, \tag{4}$$

where  $M^{\Gamma}$  is an algebraically known matrix function [15,37,38] of the lattice scattering momentum  $k(E_{\rm cms}^2) = \sqrt{E_{\rm cms}^2/4 - M_{\pi}^2}$  and the pion mass,  $M_{\pi}$ . Note that Eq. (4) is valid below inelastic threshold ( $E_{\rm cms} < 4M_{\pi}$ ) only. This represents a limitation in particular for the ensemble E132, where only five energy levels lie below this threshold for our L-value. In a more general sense this also implies that independently of the number of points below threshold, the resonance region of the  $\rho$ -meson can never be mapped out using Lüscher's method only, because  $4M_{\pi}^{\rm phys} < M_{\rho}$ . Fortunately, it is possible to include ensembles with larger than physical pion mass values. Using such ensembles at physical and heavier than physical pion mass, the IAM still allows us to obtain a result for the  $\rho$ -resonance parameters at the physical point. Only with large enough volumes available and by possibly including the  $4\pi$  channel in the analysis this shortcoming can be overcome in the future.

Given only discrete values of  $E_{\rm cms}$ , one needs to parameterise the scattering amplitude as a function of a continuous  $E_{\rm cms}$ . One example for such a parametrization is a simple Breit-Wigner (BW) form

$$\tan \delta_1^{\text{BW}}(s) = \frac{g_{\rho\pi\pi}^2}{6\pi} \frac{k^3(s)}{\sqrt{s} (M_{\rho}^2 - s)},$$
 (5)

with  $M_{\rho}$  the  $\rho$ -resonance mass,  $g_{\rho\pi\pi}$  the  $\rho-\pi\pi$  coupling, k the lattice scattering momentum defined above and s the centre-of-mass energy squared. The width  $\Gamma_{\rho}$  is related to  $M_{\rho}$  and  $g_{\rho\pi\pi}$  via

$$\Gamma_{\rho} = \frac{2}{3} \frac{g_{\rho\pi\pi}^2}{4\pi} \frac{k^3 (M_{\rho}^2)}{M_{\rho}^2} \,. \tag{6}$$

Supplementary to the experimental measurements, additional information about the dynamics of the  $\pi\pi$  system resides in the pion-mass dependence, which can be explored with lattice calculations. Being in the unique position of having data at the physical, as well as heavier than physical pion mass values, we use the IAM parametrization of the scattering amplitude [21–23]. This approach preserves unitarity exactly, has the correct pion mass dependence up to next-to-leading order (NLO) in chiral perturbation theory [39,40] and fulfils further non-perturbative constraints on the chiral trajectory [41].

In IAM, the phase-shift  $\delta_1$  is parameterised as (for more details see Ref. [18])

$$\cot \delta_1^{\text{IAM}}(s) = \frac{\sqrt{s}}{2k} \left( \frac{T_2(s) - \bar{T}_4(s)}{(T_2(s))^2} - 16\pi \text{ Re } J(s) \right), \tag{7}$$

where  $T_2$  denotes the leading chiral order amplitude and  $\bar{T}_4$  the NLO one without s-channel loop diagrams. The two-meson loop in dimensional regularisation is denoted by J(s). The corresponding amplitude is regularisation scale independent and depends on one combination of low-energy constants (LECs) [39]  $\bar{l}_{12} := \bar{l}_1 - \bar{l}_2$  as well as on the pion decay-constant in the chiral limit  $(f_0)$ . Note that both  $T_2$  and  $T_4$  are expressed in terms of  $\xi = M_\pi^2/(4\pi f_0)^2$ .

The expressions (5) and (7) are fitted directly to the energy eigenvalues using Eq. (4) without computing the phase-shift as an intermediate quantity. Since we work at a single lattice spacing value, all fits are carried out entirely in lattice units. Fit parameters are the BW parameters  $g_{\rho\pi\pi}$  and  $M_{\rho}$  or the aforementioned LECs, depending on the considered fit form. Both fit forms depend on  $M_{\pi}$ . We include our lattice values  $aM_{\pi}$  with error estimates in the fit using the procedure detailed in appendix B of Ref. [15]. In the case of the IAM, instead of simply including  $f_0$  as a fit parameter, we include our lattice estimates for  $af_{\pi}$  with error estimate in the fit by relating it to  $f_0$  via [39]

$$f_{\pi} = f_0 \left( 1 - 2\xi \log \left[ \frac{M_{\pi}^2}{\Lambda_4^2} \right] \right). \tag{8}$$

Thus, we add  $\Lambda_4$  as a fit parameter, which is related to the NLO LEC  $\bar{l}_4$  [39], but with additional data for  $f_\pi$  included in the fit. For both,  $M_\pi$  and  $f_\pi$  we correct the lattice data for finite volume effects using the parameter free ChPT predictions [42]

$$M_{\pi}(L) = M_{\pi} \left( 1 + \frac{1}{2} \xi g_1 \right),$$

$$f_{\pi}(L) = f_{\pi} (1 - 2\xi g_1),$$
(9)

with  $g_1$  as defined in Ref. [42].

In the case of single ensemble fits we use the lattice spacing estimated in Ref. [20] to express the results in physical units.

For the global IAM fit we instead use a self consistent procedure. We define the physical point using the current FLAG [43] values  $M_\pi^{\rm phys}=135$  MeV and  $f_\pi^{\rm phys}=130.41$  MeV. Next, we fit both  $\cot\delta_1^{\rm IAM}$  and  $af_\pi$  simultaneously as functions of  $(aM_\pi)^2$  with fit parameters  $\bar{l}_1-\bar{l}_2$ ,  $\bar{l}_4$  and  $af_0$ . Now, using Eq. (8) we express

$$\frac{f_{\pi}^{\text{phys}}}{M_{\pi}^{\text{phys}}} = \frac{af_0}{aM_{\pi}^{\text{phys}}} \times \left(1 - 2\left(\frac{aM_{\pi}^{\text{phys}}}{4\pi af_0}\right)^2 \log\left(\frac{(aM_{\pi}^{\text{phys}})^2}{(a\Lambda_4)^2}\right)\right), \tag{10}$$

and numerically solve for  $aM_\pi^{\rm phys}$  with fitted  $af_0$  and  $a\Lambda_4$  and  $f_\pi^{\rm phys}/M_\pi^{\rm phys}=0.966$  as input. The value of a in physical units is then obtained by setting  $M_\pi^{\rm phys}=135$  MeV. Note that this relation is valid up to the next-to-leading chiral order. We perform this for each of the bootstrap samples and methods **A1-3** separately. Besides phase-shifts and pole positions at the physical point, this also allows one to extract  $f_0$  in physical units as well as the low-energy constant of interest  $\bar{l}_4=2\log(a\Lambda_4/(aM_\pi^{\rm phys}))$ . In all fits we take full account of correlations and compute statistical uncertainties using the bootstrap. All bare data is publicly available in a data repository [44].

The procedure to set the scale outlined above via  $M_{\pi}$  and  $M_{\pi}/f_{\pi}$  has in our opinion several advantages:

- $M_{\pi}$  and  $f_{\pi}$  are naturally part of the analysis and thus, we do not need to introduce additional scale setting quantities,
- both,  $M_{\pi}$  and  $f_{\pi}$  can be estimated with high statistical accuracy and the full correlation can be taken into account,
- other mesonic quantities like  $f_K$ , which can be estimated with similar accuracy, do not yield significantly higher scale setting precision amid very similar results [20].

It is clear that any scale setting procedure employing just a single value of the lattice spacing and with only two dynamical flavors is bound to suffer from systematic biases which are beyond our control. In particular, employing a different scale setting quantity, for example the nucleon mass, would lead to a 1.2% difference in the scale and quadruple the corresponding statistical uncertainty, see Ref. [20] for details. More generally, there is an ambiguity in the scale setting procedure which can only be resolved by performing a calculation including a continuum limit and in a theory including at least three dynamical flavors. To account for these effects beyond our control, we assign a generic 2.5% uncertainty to (undetermined) discretisation artefacts which are generically of order  $a^2\Lambda_{\rm QCD}^2$  and a 1.2% scale setting uncertainty in our final results.

#### 4. Results

Here we present and discuss mainly the results obtained with method **A1** to estimate energy levels if not mentioned otherwise. For methods **A2-3** see the supplemental material. In Fig. 1 we show  $k\cot(\delta_1)$  as a function of the centre-of-mass energy  $E_{\rm cms}$  both in units of the pion mass for the three ensembles separately. The solid red lines with  $1\sigma$  error band correspond to the best fits of Eq. (7) directly to the energy levels on each ensemble separately, the blue dashed lines to Breit-Wigner fits Eq. (5). The data points with slanted error bars indicating the correlation between  $\delta_1$  and  $E_{\rm cms}$  are generated using Eq. (4) for illustration purposes only. Filled symbols correspond to data points with  $E_{\rm cms}/M_{\pi} \leq 4$ , which are included in the fits, open symbols to the rest.

The results of our fits and the corresponding  $\chi^2_{\rm dof}$  values are compiled in Table 2. The complex  $\rho$ -resonance pole position  $E_{\rho} = M_{\rho} + i\Gamma_{\rho}/2$  is found by analytical continuation of the scattering

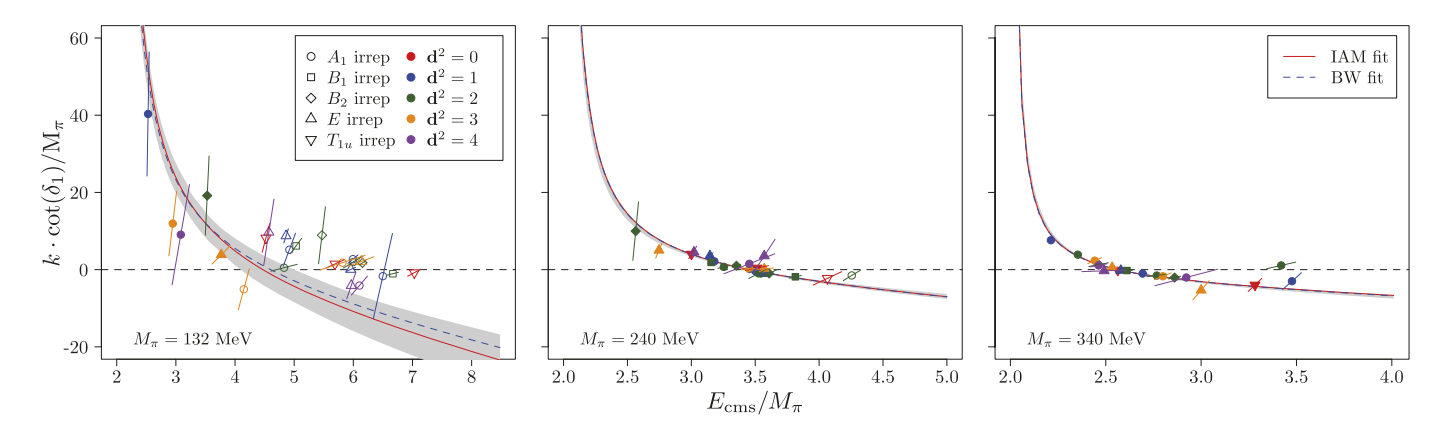


**Fig. 1.**  $k \cot(\delta_1)$  as a function of  $E_{cms}$ , both in units of  $M_\pi$ , obtained from the fits to energy eigenvalues of analysis **A1** for the three individual ensembles separately (from left to right: E132, E240 and E340). Full red (with  $1\sigma$  uncertainty band in grey) and blue dashed lines show results of IAM- and BW-based fits, respectively. Data points are added for illustration purposes only. For better legibility we have dropped a few points with absolute error larger than 20 and relative error larger than 75%. Only data points with filled symbols are included in the underlying fits.

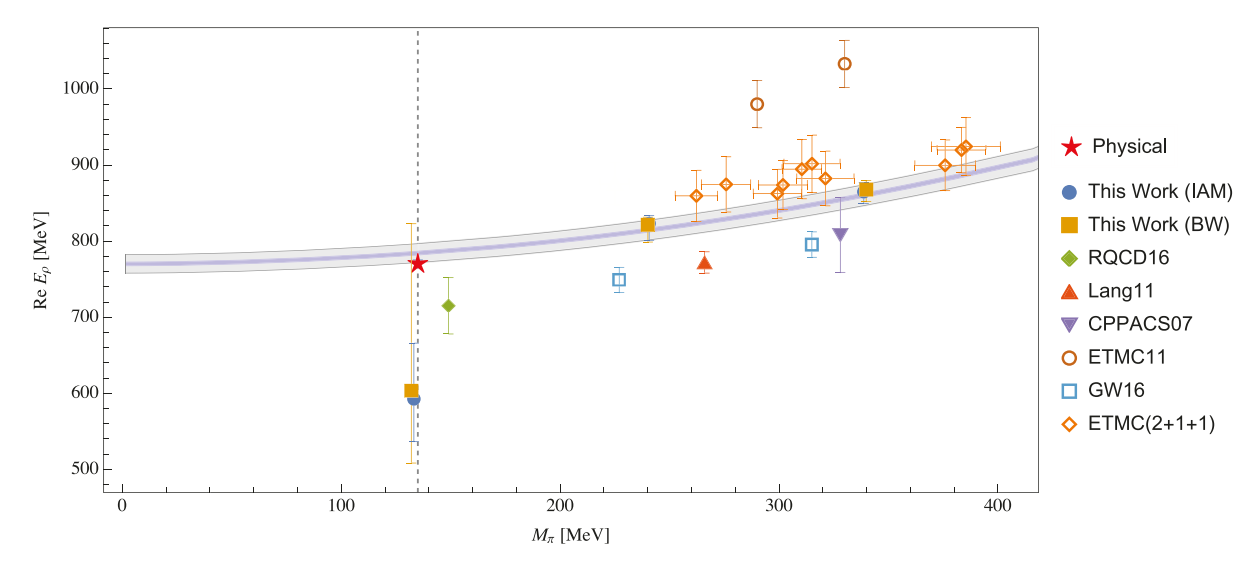


**Fig. 2.** Compilation of results of this and other  $N_f = 2$  calculations [5,6,9,45] on  $M_\rho(M_\pi)$ . Results of ETMC 2+1+1 calculation [15] are included for comparison, too. The indicated error bars combine systematic and statistical uncertainties. The blue (grey) shaded band shows the pion mass dependence of our global fit with corresponding statistical (statistical and systematic) uncertainty. We quote the PDG central value [1] by the red star at 135 MeV (dashed vertical line) for comparison.

amplitude to the complex energy-plane. Note that in the case of the BW parametrization this can also be approximated by Eq. (6), while in the case of the IAM parametrization, the poles are recoded on the second Riemann Sheet in the usual manner, see, e.g., Refs. [46–48] for explicit IAM expressions. The results are given in Table 3 in the last two columns. The last row corresponds to the result of the global IAM fit and the pole position at the physical point, determined as outlined above and resulting in a=0.0919(1) fm (statistical error only) well compatible with the result from Ref. [20]. The results of the single (IAM, BW) and global (IAM) fits are depicted in Fig. 2 together with the physical result [1] and previous  $N_f=2$  lattice determinations [5,6,9,45]. In the same figure we also show the  $N_f=2+1+1$  results of Ref. [15], because this is the only work where the continuum limit was taken.

The complex pole positions of our global fit are visualised in Fig. 3. The solid  $1\sigma$  error band represents  $E_\rho$  determined by the global IAM fit as a function of the pion mass (from larger pion mass in the bottom right to smaller pion mass in the top left corner of the plot), the blue ellipse indicates the corresponding pole position at the physical point. The two grey ellipses correspond to pole positions from global IAM fits **A2** and **A3**. In addition, we show PDG values [1], indicating the variation in the phenomeno-

**Table 2**Results of IAM-based correlated fits to single ensembles and global set of eigenvalues, including statistical uncertainties determined from re-sampling. Fits are based on energy levels estimated with method **A1**, for **A2-3** see [34].

Ens	$\bar{l}_{12}$	$af_0$	$a\Lambda_4$	$\chi^2_{dof}$	dof
E132	$-11.0^{+2.5}_{-2.8}$	$0.060^{+0.002}_{-0.003}$	$0.088^{+0.284}_{-0.067}$	1.6	4
E240	$-6.8  ^{+0.8}_{-0.4}$	$0.065^{+0.002}_{-0.004}$	$0.138^{+0.167}_{-0.039}$	0.9	25
E340	$-6.3  ^{+0.2}_{-0.8}$	$0.063^{+0.004}_{-0.001}$	$0.041^{+0.041}_{-0.104}$	0.8	23
all	$-5.3 ^{\ +0.0}_{\ -0.1}$	$0.057^{+0.000}_{-0.000}$	$0.543^{+0.010}_{-0.006}$	1.1	58

logical extractions, and results of chiral extrapolations of previous heavier pion mass  $N_f = 2$  lattice determinations [9,16,18].

Finally, in Fig. 4 we show the experimental phase-shift data [2, 3] as a function of  $E_{\rm cms}$  and compare to our global IAM fit prediction for the physical pion mass value. For the latter we plot in blue the envelope area of all the error bands of the three global IAM analyses **A1-3**, thus, visualising statistical and IAM uncertainties. The grey band includes our estimate of the lattice artefacts and the scale setting uncertainty added in quadrature. The lattice

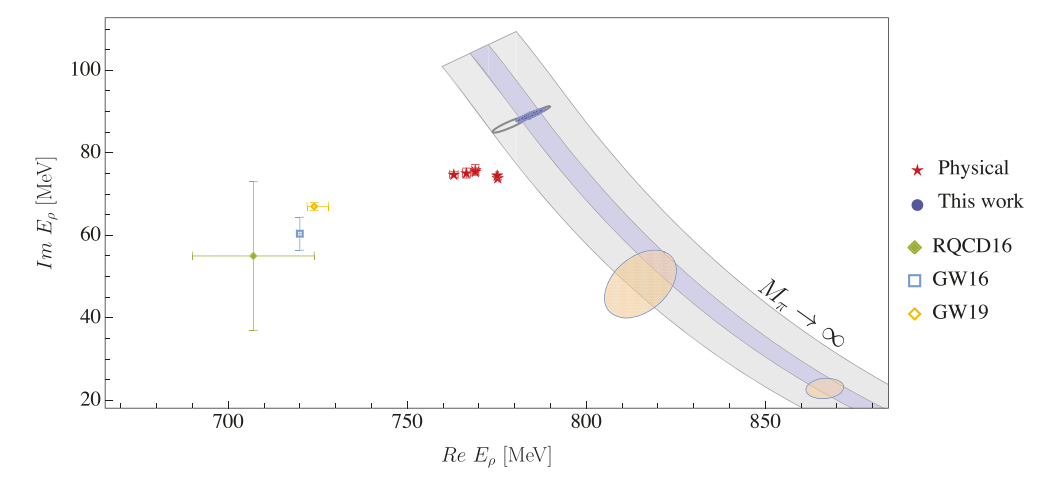


**Fig. 3.** The complex pole position of the  $\rho$ -meson. The blue ellipse shows the  $1\sigma$  boundary of the pole positions (global fit **A1**) at the physical point. Corresponding ellipses for global fits to methods **A2-3** are depicted as grey empty ellipses. Blue (grey) shaded band shows the pion mass dependence of the pole position with corresponding  $1\sigma$  statistical (statistical and systematic) uncertainty. PDG results [1] and those of earlier lattice calculations [9,16,18] are quoted for comparison. Light orange ellipses correspond to individual fits for the two ensembles at unphysically large pion mass values.

**Table 3** Pole positions  $E_{\rho}$  determined using IAM and BW parametrizations for the different lattice ensembles with method **A1** to estimate the energy levels. Last row shows the extrapolation of the global IAM fit to the physical point.

Ens	Method	$\operatorname{Re} E_{\rho} [\operatorname{MeV}]$	$\operatorname{Im} E_{\rho} [\operatorname{MeV}]$
E132	IAM	$587.3^{+65.7}_{-49.1}$	$28.8^{+14.1}_{-8.7}$
	BW	$603.1^{+228.2}_{-86.9}$	$34.2^{+171.9}_{-24.3}$
E240	IAM	$821.0_{-11.8}^{+0.0}$	$48.0_{-4.1}^{+5.0}$
	BW	$821.0_{-11.8}^{+0.0}$	$48.0_{-4.1}^{+5.0}$
E340	IAM	$868.0^{+1.7}_{-5.4}$	$24.1_{-2.7}^{+0.3}$
	BW	$868.0^{+1.7}_{-5.8}$	$24.1_{-2.7}^{+0.3}$
all	global IAM	$786.8^{+0.1}_{-5.2}$	$90.1_{-2.0}^{+0.0}$

prediction agrees with most of the experimental points within two  $\sigma$ .

#### 5. Discussion

First, we observe very good agreement between BW and IAM fits on the three ensembles separately, as can be see in Tables 2 and 3, with smaller errors in the IAM fits. This is even the case on the physical point ensemble, however, with much too low pole mass and width. The latter can be attributed to only five points which can be included in the fit. These five points for the phase shift are all located at values of  $E_{\rm cms}$  where the phase shift  $\delta_1$  is close to zero. This leads to the situation that mostly a single point at the largest included value of  $E_{\rm cms}$  is determining the curvature, as can also be seen in the leftmost panel of Fig. 1. If this single phase shift value was lower by one  $\sigma$ , the result of the single ensemble fit would change significantly. Insofar, we conclude that systematic errors of such fits to the phase shift with insufficiently many data points in the resonance region are underestimated.

This emphasises the importance of including ensembles with larger than physical pion mass value in the analysis: only on those ensembles can the Lüscher method cover the resonance region fully.

Interestingly, if one were to ignore the inelastic threshold on the physical point ensemble and use Eq. (4) to obtain values for  $\delta_1$ , the such obtained phase-shift points compare better with the

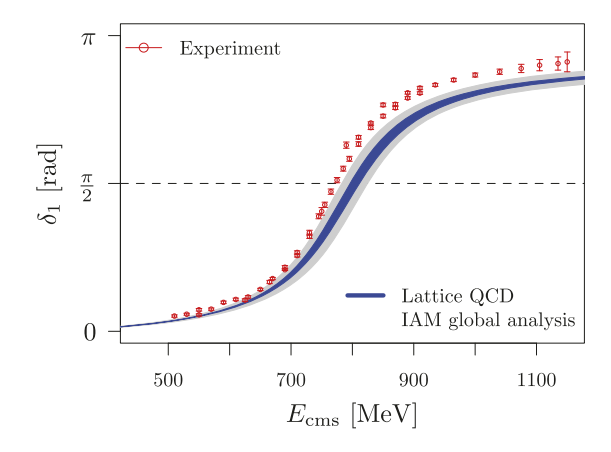


**Fig. 4.**  $\rho$ -meson p-wave phase-shift  $\delta_1$  at the physical point. We compare experimental data [2,3] to our prediction from three global IAM fits to  $N_f=2$  lattice QCD data, see text. The blue band visualises the statistical and fitting uncertainties, the grey band includes in addition the estimated lattice artefacts and scale setting uncertainty added in quadrature.

experimental data than the results from our single ensemble fits restricted to energy values below inelastic threshold. In particular, the resonance masses are for these fits 50-80 MeV larger than the PDG value. This better agreement is likely due to the fact that  $\rho \to \pi\pi$  is almost elastic up to 1 GeV, which is actually also the assumption to obtain the experimental phase-shift points (see also Ref. [49]). We decided not to include such fits in our main analysis, because it adds in our opinion uncontrolled systematics rendering the results difficult to interpret. However, the corresponding pole positions can be found in the supplemental material.

The three global IAM analyses based on energy determinations A1-3 agree very well with each other (see Tab. 1 in [34]) and we conclude that they lead to consistent chiral extrapolations. Though the physical point ensemble E132 might not, due to the few energy levels, add much information to the global fit, it anchors the fit at slightly below the physical pion mass value.

Below, we take the maximum of the  $\pm$  statistical errors as our statistical uncertainty, the maximal deviation between the three analyses **A1-3** as a systematic uncertainty. Therefore, we quote as our final result the results from the global IAM fit with analysis method **A1**, reading

$$\begin{split} M_{\rho} &= 786 \ (5)_{\text{stat}} \ (1)_{\text{sys}} \ (19)_{\text{lat}} \ (10)_{\text{scale}} \ \text{MeV} \,, \\ \Gamma_{\rho} &= 180 \ (4)_{\text{stat}} \ (1)_{\text{sys}} \ (5)_{\text{lat}} \ (2)_{\text{scale}} \ \text{MeV} \,, \\ \bar{l}_{12} &= -5.27 \ (8)_{\text{stat}} \ (3)_{\text{sys}} \ (13)_{\text{lat}} \ (6)_{\text{scale}} \,, \\ \bar{l}_{4} &= +4.31 \ (4)_{\text{stat}} \ (2)_{\text{sys}} \ (11)_{\text{lat}} \ (5)_{\text{scale}} \,, \\ f_{0} &= 122.27 \ (8)_{\text{stat}} \ (4)_{\text{sys}} \ (3.06)_{\text{lat}} \ (1.47)_{\text{scale}} \ \text{MeV} \,. \end{split}$$

Note that our parametrically estimated lattice artefacts are the largest source of uncertainty in our results.

In the past, other calculations of the isovector  $\pi\pi$  scattering with two dynamical quarks have been performed as well. The goal of these and the present study is to clarify the role of the strange quark in the simplest hadronic resonance channel, which is complimentary information to any experimental data and thus may lead to a deeper understanding of the QCD dynamics. Specifically, it was believed that the strange quark plays only a minor to no role for this channel, which then was challenged by the GWUQCD result [12] and following chiral extrapolations to the physical point [16,17,50]. Based on a chiral unitary approach different from ours, it was reported there that the two-flavor  $\rho$ -resonance is lighter than the physical one by about 50 MeV and that the missing strangeness channels might explain this discrepancy. Later, more sophisticated extrapolations were performed in Refs. [18,19] confirming the lighter  $\rho$ -mass at the physical point.

In contrast to this, our results are much closer to the values quoted in the PDG, even though obtained using an approach for the chiral extrapolation similar to Ref. [18,19]. There are different possibilities to explain this difference: on the one hand a reason for the difference could be, as suggested in Ref. [19], the scale setting procedure. The scale setting for our ensembles using various different observables is discussed comprehensively in Ref. [20]. The 1.2% change when using the nucleon mass instead of  $f_{\pi}$  to set the scale would indeed shift our result towards lower values for  $M_{\rho}$  (if applied blindly by not taking the corresponding change in  $M_{\pi}$  into account), but not enough to obtain values as low as reported in Ref. [12]. Also, as mentioned above, errors would increase significantly at the same time. Using the gradient flow scale  $w_0$  determined in Ref. [20] (again blindly) would induce an even larger shift. Here, the physical value for  $w_0$  with  $N_f = 2$  is taken from the proceeding contribution [51]. The scale determination from  $w_0$ , however, appears to be an outlier, since even using the alternative gradient flow scale  $\sqrt{t_0}$  leads to results completely in line with the scales determined from  $f_{\pi}$ .

On the other hand, a difference could also come from lattice artefacts, which we cannot control in our calculation, nor are we aware of a continuum extrapolation of the  $\rho$ -resonance properties in  $N_f=2$  flavour lattice QCD. Thus, lattice artefacts could provide the additional shift to bring our result to agreement with a significantly lower  $\rho$ -resonance mass value. But also the other  $N_f=2$  flavour lattice results could be affected by such artefacts.

Compared to Ref. [15] with  $N_f=2+1+1$  dynamical quark flavours, we have presented in this letter a significantly better controlled chiral extrapolation thanks to the included physical point ensemble and the IAM. While the pole mass is similarly close to the experimental value, our width is larger than the experimental one, whereas in Ref. [15] a lower value was found. A final estimate will require a continuum extrapolation at the physical pion mass value.

When one compares the results presented here for the  $N_f=2$  ensembles at larger than physical pion mass value to the corresponding results with  $N_f=2+1+1$  from Ref. [15] directly in Fig. 2, one observes a systematic downward trend from  $N_f=2+1+1$  to  $N_f=2$  in the  $\rho$ -resonance mass values. As mentioned above, this could be due to scale setting, residual lattice artefacts, or simply statistics. We cannot exclude with certainty that the

 $N_f = 2$  flavour  $\rho$ -resonance mass is lower than its  $N_f = 2 + 1 + 1$  counter part.

#### 6. Conclusion

We have presented a lattice QCD analysis of the  $\rho$ -resonance including an ensemble with slightly lower than physical pion mass value for the first time. This allows us to estimate the  $\rho$ -resonance parameters at the physical point using the inverse amplitude method including the pion mass dependence up to NLO in the chiral expansion.

With all our uncertainties added in quadrature, our results for the  $\rho$ -resonance mass and width read

$$M_{\rho} = 786(22) \text{ MeV}, \quad \Gamma_{\rho} = 180(6) \text{ MeV}.$$

While  $M_{\rho}$  agrees well with the PDG value, the width is too large by 20%. The low energy constants are in very good agreement with the corresponding FLAG lattice averages [43,52–56]. This is not necessarily expected, since the IAM resums higher order effects due to unitarisation. While comparing with experiment, it is important to keep in mind that our calculation is based on  $N_f=2$  dynamical quark flavours, which introduces a systematic uncertainty we cannot control.

Our result for the resonance mass is in good agreement with experiment, even though the  $K\bar{K}$  threshold is not present. This difference to previous  $N_f=2$  lattice calculations can still be explained by (a combination of) scale setting and lattice artefacts.

We summarise the result of this letter in Fig. 4, where, in addition to the experimental data for the *p*-wave phase-shift, the blue band shows our result for the phase-shift at the physical pion mass value obtained from the global IAM fit. The width of the band represents fitting and statistical uncertainties. The grey band includes in addition an estimate of lattice artefacts and scale setting uncertainty.

Eventually, this computation needs to be repeated with  $N_f = 2 + 1(+1)$  dynamical quark flavours, several values of the lattice spacing and physical point ensembles included. Particular emphasis should also be on different spatial volumes at the physical point.

## **Declaration of competing interest**

The authors declare that they have no known competing financial interests or personal relationships that could have appeared to influence the work reported in this paper.

### Acknowledgements

We thank all members of the ETMC for the most enjoyable collaboration. The authors gratefully acknowledge the Gauss Centre for Supercomputing e.V. (www.gauss-centre.eu) for funding this project by providing computing time on the GCS Supercomputer JUQUEEN [57] and the John von Neumann Institute for Computing (NIC) for computing time provided on the supercomputers JU-RECA [58] and JUWELS [59] at Jülich Supercomputing Centre (JSC). We thank Ulf-G. Meißner for useful comments on the manuscript. This project was funded in part by the DFG as a project in the Sino-German CRC110. FP acknowledges financial support from the Cyprus Research and Innovation Foundation under project "NextQCD", contract no. EXCELLENCE/0918/0129. The open source software packages tmLQCD [60-62], Lemon [63], QUDA [64-66], the hadron package [67] and R [68] have been used. MM thanks R. Brett and A. Alexandru for assistance in implementation of Fin-Vol routines.

#### Appendix A. Supplementary material

Supplementary material related to this article can be found online at https://doi.org/10.1016/j.physletb.2021.136449.

#### References

- [1] PDG Collaboration, M. Tanabashi, et al., Phys. Rev. D 98 (2018) 030001, https://link.aps.org/doi/10.1103/PhysRevD.98.030001.
- [2] P. Estabrooks, A.D. Martin, Nucl. Phys. B 79 (1974) 301.
- [3] S.D. Protopopescu, et al., Phys. Rev. D 7 (1973) 1279.
- [4] U.-G. Meißner, Phys. Rep. 161 (1988) 213.
- [5] X. Feng, K. Jansen, D.B. Renner, Phys. Rev. D 83 (2011) 094505, arXiv:1011.5288 [hep-lat].
- [6] C.B. Lang, D. Mohler, S. Prelovsek, M. Vidmar, Phys. Rev. D 84 (2011) 054503, arXiv:1105.5636 [hep-lat];
  - C.B. Lang, D. Mohler, S. Prelovsek, M. Vidmar, Erratum, Phys. Rev. D 89 (5) (2014) 059903.
- [7] CS Collaboration, S. Aoki, et al., Phys. Rev. D 84 (2011) 094505, arXiv:1106.5365 [hep-lat].
- [8] Hadron Spectrum Collaboration, J.J. Dudek, R.G. Edwards, C.E. Thomas, Phys. Rev. D 87 (2013) 034505, arXiv:1212.0830 [hep-ph]; Hadron Spectrum Collaboration, J.J. Dudek, R.G. Edwards, C.E. Thomas, Erratum,
- Phys. Rev. D 90 (9) (2014) 099902.

  [9] RQCD Collaboration, G.S. Bali, et al., Phys. Rev. D 93 (2016) 054509, arXiv:1512.
- 08678 [hep-lat].
  [10] D.J. Wilson, R.A. Briceno, J.J. Dudek, R.G. Edwards, C.E. Thomas, Phys. Rev. D 92
- (2015) 094502, arXiv:1507.02599 [hep-ph].
- [11] Z. Fu, L. Wang, Phys. Rev. D 94 (2016) 034505, arXiv:1608.07478 [hep-lat].
- [12] D. Guo, A. Alexandru, R. Molina, M. Döring, Phys. Rev. D 94 (2016) 034501, arXiv:1605.03993 [hep-lat].
- [13] C. Alexandrou, et al., Phys. Rev. D 96 (2017) 034525, arXiv:1704.05439 [hep-lat].
- [14] C. Andersen, J. Bulava, B. Hörz, C. Morningstar, Nucl. Phys. B 939 (2019) 145, arXiv:1808.05007 [hep-lat].
- [15] ETM Collaboration, M. Werner, et al., Eur. Phys. J. A 56 (2020) 61, arXiv:1907. 01237 [hep-lat].
- [16] R. Molina, D. Guo, B. Hu, A. Alexandru, M. Döring, EPJ Web Conf. 137 (2017) 05019, arXiv:1611.04536 [hep-lat].
- [17] B. Hu, R. Molina, M. Döring, M. Mai, A. Alexandru, Phys. Rev. D 96 (2017) 034520, arXiv:1704.06248 [hep-lat].
- [18] M. Mai, C. Culver, A. Alexandru, M. Döring, F.X. Lee, Phys. Rev. D 100 (2019) 114514, arXiv:1908.01847 [hep-lat].
- [19] R. Molina, J. Ruiz de Elvira, J. High Energy Phys. 11 (2020) 017, arXiv:2005. 13584 [hep-lat].
- [20] ETM Collaboration, A. Abdel-Rehim, et al., Phys. Rev. D 95 (2017) 094515, arXiv:1507.05068 [hep-lat].
- [21] T.N. Truong, Phys. Rev. Lett. 61 (1988) 2526.
- [22] A. Dobado, J.R. Pelaez, Phys. Rev. D 56 (1997) 3057, arXiv:hep-ph/9604416 [hep-ph].
- [23] A. Gomez Nicola, J.R. Pelaez, G. Rios, Phys. Rev. D 77 (2008) 056006, arXiv: 0712.2763 [hep-ph].
- [24] Y. Iwasaki, Nucl. Phys. B 258 (1985) 141.
- [25] Alpha Collaboration, R. Frezzotti, P.A. Grassi, S. Sint, P. Weisz, J. High Energy Phys. 08 (2001) 058, arXiv:hep-lat/0101001 [hep-lat].
- [26] R. Frezzotti, G.C. Rossi, Nucl. Phys. Proc. Suppl. 128 (2004) 193, arXiv:hep-lat/ 0311008 [hep-lat], (2003) 193.
- [27] R. Frezzotti, G.C. Rossi, J. High Energy Phys. 08 (2004) 007, arXiv:hep-lat/ 0306014.
- [28] C. Michael, I. Teasdale, Nucl. Phys. B 215 (1983) 433.
- [29] M. Lüscher, U. Wolff, Nucl. Phys. B 339 (1990) 222.

- [30] M. Fischer, et al., arXiv:2004.10472 [hep-lat].
- [31] C. Morningstar, et al., Phys. Rev. D 83 (2011) 114505, arXiv:1104.3870 [hep-lat].
- [32] P. Dimopoulos, et al., Phys. Rev. D 99 (2019) 034511, arXiv:1812.08787 [hep-lat]
- [33] ETM Collaboration, P. Boucaud, et al., Comput. Phys. Commun. 179 (2008) 695, arXiv:0803.0224 [hep-lat].
- [34] See Supplemental Material at [URL will be inserted by publisher]
- [35] M. Lüscher, Commun. Math. Phys. 105 (1986) 153.
- [36] M. Lüscher, Nucl. Phys. B 354 (1991) 531.
- [37] J. Bulava, et al., Nucl. Phys. B 910 (2016) 842, arXiv:1604.05593 [hep-lat].
- [38] C. Morningstar, et al., Nucl. Phys. B 924 (2017) 477, arXiv:1707.05817 [hep-lat].
- [39] J. Gasser, H. Leutwyler, Ann. Phys. 158 (1984) 142.
- [40] J. Gasser, H. Leutwyler, Nucl. Phys. B 250 (1985) 465.
- [41] P.C. Bruns, M. Mai, Phys. Lett. B 778 (2018) 43, arXiv:1707.08983 [hep-lat].
- [42] J. Gasser, H. Leutwyler, Phys. Lett. B 184 (1987) 83.
- [43] FLAG Collaboration, S. Aoki, et al., arXiv:1902.08191 [hep-lat].
- [44] M. Fischer, et al., Data repository, https://github.com/urbach/datarhonf2.
- [45] S. Aoki, et al., Eur. Phys. J. C 74 (2014) 2890, arXiv:1310.8555 [hep-lat].
- [46] C. Hanhart, J. Pelaez, G. Rios, Phys. Rev. Lett. 100 (2008) 152001, arXiv:0801. 2871 [hep-ph].
- [47] N.R. Acharya, F.-K. Guo, M. Mai, U.-G. Meißner, Phys. Rev. D 92 (2015) 054023, arXiv:1507.08570 [hep-ph].
- [48] M. Döring, B. Hu, M. Mai, Phys. Lett. B 782 (2018) 785, arXiv:1610.10070 [hep-lat].
- [49] J. Gasser, U.G. Meißner, Nucl. Phys. B 357 (1991) 90.
- [50] B. Hu, R. Molina, M. Döring, A. Alexandru, Phys. Rev. Lett. 117 (2016) 122001, arXiv:1605.04823 [hep-lat].
- [51] ALPHA Collaboration, M. Bruno, R. Sommer, PoS LATTICE 2013 (2014) 321, arXiv:1311.5585 [hep-lat].
- [52] ETM Collaboration, R. Frezzotti, V. Lubicz, S. Simula, Phys. Rev. D 79 (2009) 074506, arXiv:0812.4042 [hep-lat].
- [53] ETM Collaboration, R. Baron, et al., J. High Energy Phys. 08 (2010) 097, arXiv: 0911.5061 [hep-lat].
- [54] B.B. Brandt, A. Jüttner, H. Wittig, J. High Energy Phys. 11 (2013) 034, arXiv: 1306.2916 [hep-lat].
- [55] V. Gülpers, G. von Hippel, H. Wittig, Eur. Phys. J. A 51 (2015) 158, arXiv:1507. 01749 [hep-lat].
- [56] G.P. Engel, L. Giusti, S. Lottini, R. Sommer, Phys. Rev. D 91 (2015) 054505, arXiv: 1411.6386 [hep-lat].
- [57] Jülich Supercomputing Centre, J. Large-Scale Res. Facil. 1 (2015), https://doi.org/ 10.17815/jlsrf-1-18.
- [58] Jülich Supercomputing Centre, J. Large-Scale Res. Facil. 4 (2018), https://doi.org/ 10.17815/jlsrf-4-121-1.
- [59] Jülich Supercomputing Centre, J. Large-Scale Res. Facil. 5 (2019), https://doi.org/ 10.17815/jlsrf-5-171.
- [60] K. Jansen, C. Urbach, Comput. Phys. Commun. 180 (2009) 2717, arXiv:0905. 3331 [hep-lat].
- [61] A. Abdel-Rehim, et al., PoS LATTICE 2013 (2014) 414, arXiv:1311.5495 [hep-lat].
- [62] A. Deuzeman, K. Jansen, B. Kostrzewa, C. Urbach, PoS LATTICE 2013 (2013) 416, arXiv:1311.4521 [hep-lat].
- [63] ETM Collaboration, A. Deuzeman, S. Reker, C. Urbach, Comput. Phys. Commun. 183 (2012) 1321, arXiv:1106.4177 [hep-lat].
- [64] M.A. Clark, R. Babich, K. Barros, R.C. Brower, C. Rebbi, Comput. Phys. Commun. 181 (2010) 1517, arXiv:0911.3191 [hep-lat].
- [65] R. Babich, et al., Scaling lattice QCD beyond 100 GPUs, in: SC11, Washington, November 12–18, 2011, 2011, arXiv:1109.2935 [hep-lat].
- [66] M.A. Clark, et al., arXiv:1612.07873 [hep-lat].
- [67] B. Kostrzewa, J. Ostmeyer, M. Ueding, C. Urbach, Hadron: Analysis Framework for Monte Carlo Simulation Data in Physics, 2020, R package version 3.1.0.
- [68] R Development Core Team, R: A language and environment for statistical computing, in: R Foundation for Statistical Computing, Vienna, Austria, ISBN 3-900051-07-0, 2005.